Coupled Space-Marching Method for the Navier-Stokes Equations for Subsonic Flows

P. W. TenPas*
University of Kansas, Lawrence, Kansas 66045
and
R. H. Pletcher†
Iowa State University, Ames, Iowa 50011

An implicit space-marching finite-difference procedure is described for solving the compressible form of the steady, two-dimensional Navier-Stokes equations in body-fitted curvilinear coordinates. The coupled system of equations is solved for the primitive variables of velocity and pressure by making multiple sweeps of the space-marching procedure. A new pressure correction method has been developed that significantly accelerates convergence of the iterative process. The scheme is used to compute incompressible flows by taking the low Mach number limit of the compressible formulation. Computed results are compared with other numerical predictions for low Reynolds number channel inlet flow, flow over a rearward-facing step in a channel, and external flow over a cylinder.

Introduction

A NUMBER of different methods have been developed to solve the Navier-Stokes equations in primitive variables for steady, subsonic flows. Many of these algorithms are described in Anderson et al.[1] The present methods are not entirely adequate for all problems, and advanced techniques continue to be developed. New procedures and recent improvements to existing methods are briefly reviewed in the following paragraphs.

The most frequently used primitive variable algorithms for incompressible flows solve the momentum equations for the velocity components in an uncoupled (segregated) manner, holding pressure fixed. Although different in detail, the segregated solution schemes (e.g., Refs. 2–4) use the continuity equation indirectly in the formulation of a separate Poisson equation that is solved for the pressure. Since the velocity components and pressure are computed from different algorithms, rather than in a coupled manner, convergence is slowed. Furthermore, the solution of the elliptic Poisson equation consumes a large part of the total computaion time for each global iteration. Van Doormaal et al.[5] recently have evaluated improved algorithms for solving the pressure Poisson equation, and Rhie[4] has applied a multigrid method to accelerate the solution of the momentum equations and the pressure equation.

Several strategies have been advanced for solving the coupled momentum and continuity equations for the primitive variables, including the pressure. The schemes all share the advantage that a separate procedure for imposing the continuity constraint and determining the pressure is not required. The choice of variables and the algebraic approach used to solve the system of nonlinear equations distinguish the direct, time-marching, and space-marching algorithms.

Vanka and Leaf[6] and recently Patankar et al.[7] have compared solutions for two-dimensional flows obtained by direct and segregated methods. A large sparse matrix solver is used to invert a system of equations spanning the entire flow domain. Multiple inversions are required to converge the nonlinear and type-dependent coefficients. Although the computational effort per iteration is large, the total processing time is reduced since relatively few iterations are needed.

Most time-marching algorithms use density as a primary variable and do not perform well in the incompressible limit. To overcome this problem, Kwak et al.[8] have used a pseudo-compressibility[9] formulation of the incompressible Navier-Stokes equations in two and three dimensions. The Beam-Warming[10] differencing strategy requires solution of a set of equations along each grid line for each spatial dimension at each pseudo-timestep.

Space-marching algorithms sweep the flow domain in only one spatial direction, preferably the main streamwise flow direction. Multiple sweeps are executed to resolve the downstream effects of elliptic flows. Coupled space-marching algorithms for reduced forms of the Navier-Stokes equations for incompressible or subsonic flow have been developed by Rubin and Reddy,[11] Israeli and Lin,[12] Pougare and Lakshminarayana,[13] and Liu and Pletcher.[14] Recently, Bentson and Vradis[15] have presented solutions of the full Navier-Stokes equations in incompressible form.

In general, there appears to be broad interest in the development of advanced procedures for subsonic flows, especially for those that hold promise for extension to three-dimensional flows and to the supersonic regime. It is not yet clear which overall approach is best, and selection of a workable algorithm remains problem dependent.

In particular, the coupled space-marching algorithm is in an early stage of development. This paper contributes a different, more general formulation incorporating features that permit efficient solution of a broad class of problems. First, the compressible formulation using pressure, rather than density, as a primary variable applies to incompressible as well as compressible flow regimes. The incompressible results reported here have been computed to validate the method by comparison with other known solutions before proceeding to the development of a fully compressible version. Second, the discretization on a regular grid in generalized curvilinear coordinates is applicable to a wide range of geometries. Finally, a new pressure correction scheme has been developed that significantly improves the convergence rate.

This paper describes the new formulation and presents the results of several example computations to demonstrate the capabilities of the method.

Received May 4, 1987; revision received Feb. 2, 1990.

*Assistant Professor, Department of Mechanical Engineering.
†Professor, Department of Mechanical Engineering. Member AIAA.

Governing Equations

The steady, compressible, two-dimensional, Cartesian coordinate form of the Navier-Stokes equations and the continuity equation can be expressed in dimensionless vector form in terms of the primitive variables as

$$\frac{\partial E}{\partial x}(q) + \frac{\partial F}{\partial y}(q) = 0 \tag{1}$$

where

$$E = \begin{bmatrix} \rho u^2 + p - \tau_{xx} \\ \rho uv - \tau_{xy} \\ \rho u \end{bmatrix}, \quad F = \begin{bmatrix} \rho uv - \tau_{yx} \\ \rho v^2 + p - \tau_{yy} \\ \rho v \end{bmatrix}, \quad q = \begin{bmatrix} u \\ v \\ p \end{bmatrix}$$

and

$$\tau_{xx} = \frac{2}{3}\frac{\mu}{Re}\left(2\frac{\partial u}{\partial x} - \frac{\partial v}{\partial y}\right)$$

$$\tau_{yy} = \frac{2}{3}\frac{\mu}{Re}\left(2\frac{\partial v}{\partial y} - \frac{\partial u}{\partial x}\right)$$

$$\tau_{xy} = \tau_{yx} = \frac{\mu}{Re}\left(2\frac{\partial u}{\partial y} + \frac{\partial v}{\partial x}\right)$$

Fluid property relationships are needed to complete the model. A procedure for general compressible flows must include the full energy equation in the set of equations. For the adiabatic, low Mach number cases considered here, the energy equation has been reduced to an algebraic equation for constant total temperature:

$$T_0 = T + (u^2 + v^2)/2c_p \tag{2}$$

The density in Eq. (1) is evaluated using the perfect gas law in combination with Eq. (2) to give

$$\rho = p/R\left[T_0 - (u^2 + v^2)/2c_p\right] \tag{3}$$

For purely incompressible flow, a constant density would be specified. Laminar flow is assumed and the viscosity is determined by the Sutherland formula:

$$\mu = C_1 T^{3/2}(1 + C_2)/(T + C_2) \tag{4}$$

Boundary conditions complete the mathematical formulation. These are described in a later section in conjunction with the numerical solution.

The preceding dimensionless variables are defined in the following manner (dimensional quantities are indicated by a tilde)

$$x = \tilde{x}/\tilde{L} \qquad y = \tilde{y}/\tilde{L} \qquad \rho = \tilde{\rho}/\tilde{\rho}_r$$

$$u = \tilde{u}/\tilde{u}_r \qquad v = \tilde{v}/\tilde{u}_r \qquad p = \tilde{p}/(\tilde{\rho}_r \tilde{u}_r^2)$$

$$T = \tilde{T}/\tilde{T}_r \qquad \mu = \tilde{\mu}/\tilde{\mu}_r \qquad R = \tilde{R}\tilde{T}_r/\tilde{u}_r^2$$

$$c_p = R\gamma/(\gamma - 1) \qquad C_1 = \tilde{C}_1/\tilde{C}_1 = 1 \qquad C_2 = \tilde{C}_2/\tilde{T}_r$$

$$Re = \tilde{\rho}_r \tilde{u}_r \tilde{L}/\tilde{\mu}_r$$

Here, L is a flowfield characteristic length, x and y the Cartesian coordinates, u and v the respective Cartesian velocity components, ρ the density, p the static pressure, μ the dynamic viscosity, T the static temperature, R the gas constant, c_p the constant pressure specific heat, γ the specific heat ratio, C_1 and C_2 the Sutherland constants, and Re the Reynolds number. The subscript r denotes the reference properties that are the upstream bulk properties for internal flow cases, or the free-stream properties for external flow cases.

Solution Procedure

For subsonic flow, the system of partial differential equations [Eq. (1)] is elliptic in the spatial coordinates and is not well posed as an initial value problem for solution by a single marching sweep. However, proper treatment of the streamwise derivative terms permits a stable space-marching calculation to be executed (see Refs. 11-14). Solution to the fully elliptic equations is accomplished by repeated global iterations of the space-marching procedure.

The present solution algorithm consists of two distinct procedures that are executed for each global iteration:

1) An implicit, block-tridiagonal, finite-difference formulation of Eq. (1) is solved for the primitive variables q at each station, starting from given upstream conditions and marching downstream.

2) An approximate pressure Poisson equation is solved for corrections to the pressure field by a line solver, sweeping upstream from the downstream boundary.

Two important considerations in the formulation of the method are discussed in the following paragraphs. The details of the numerical solution are then presented in the next section.

To insure stability in the space-marching sweep, the terms that transmit information about the condition of the downstream flow are treated as source terms, i.e., the downstream values are lagged. The downstream pressure controls the flow solution through the streamwise pressure gradient terms. This is mathematically imposed by satisfying the Vigneron[16] stability condition, which requires that the streamwise pressure gradient be forward differenced for the low Mach number flows considered in this paper. Downstream velocities may also influence the solution through the streamwise convection and diffusion terms. Where the streamwise velocity is positive, the streamwise convection terms are determined using upstream values. However, where the flow reverses, the streamwise convection terms in the momentum equations must include downstream velocities. This is accomplished by reversing the direction of the upwind differencing. Finally, downstream velocities are lagged in the streamwise viscous terms. It is emphasized that all elliptic terms are retained and that the restrictions are applied to maintain the numerical stability of the space-marching calculation.

For a large class of problems, the regions of flow recirculation are limited and the streamwise viscous stresses are small. For these conditions, the downstream influence is felt primarily through the pressure field, which is the limiting factor in the convergence of the algorithm. The pressure field may be determined solely by repeated marching sweeps. However, this approach may require a large number of iterations. Since downstream pressure signals are only passed one station upstream for each global iteration, as many iterations as there are marching stations must elapse before the downstream boundary pressure is felt at the inlet. The global pressure correction procedure is used to accelerate the convergence of the pressure field by rapidly transmitting pressure signals upstream. Since no correction is made to the velocities, the effectiveness of the pressure acceleration method will diminish for problems with significant downstream convection or diffusion terms.

Numerical Solution

Regular Computational Grid Layout in Generalized Coordinates

To simplify the treatment of arbitrary geometries, a generalized independent variable transformation is employed to map the physical grid onto a uniformly spaced computational grid. The coordinate transformation is of the form

$$\xi = \xi(x,y), \qquad \eta = \eta(x,y)$$

The metrics of the transformation are

$$\xi_x/J = y_\eta, \quad \xi_y/J = -x_\eta, \quad \eta_x/J = -y_\xi, \quad \eta_y/J = x_\xi \tag{5}$$

and the Jacobian is given by

$$J = \frac{\partial(\xi,\eta)}{\partial(x,y)} = \xi_x\eta_y - \eta_x\xi_y = 1/(x_\xi y_\eta - x_\eta y_\xi) \tag{6}$$

The continuous flowfield is approximated by values at discrete points on a mesh formed by lines of constant ξ and η (see Fig. 1). On the regular grid, all flow variables are considered to be located at the node points. Execution of the space-marching solver requires full storage for the Cartesian coordinates, velocity components, and pressure. An additional pressure value is also stored to implement the global pressure correction algorithm.

Finite-Difference Equations

The transformed governing equations may be cast in several forms. Geometric considerations associated with these forms have been examined by Hindman.[17] The strong-conservation-law form is used for the continuity equation to guarantee global conservation of mass free of truncation errors. This requires that special metrics be determined in a manner consistent with the finite-difference method. However, use of this form for the type-dependent terms in the momentum equations would require several different evaluations of the metrics. Constraints on the metric terms are avoided by using the chain-rule-conservation-law form for the momentum equations with the metrics computed using the central difference form of Eqs. (5). The Jacobian is obtained from the metrics by Eq. (6).

Momentum Equations

The governing equations [Eq. (1)] can be transformed and expressed in chain-rule-conservation-law form as

$$\frac{\xi_x}{J}\frac{\partial \boldsymbol{E}}{\partial \xi} + \frac{\xi_y}{J}\frac{\partial \boldsymbol{F}}{\partial \xi} + \frac{\eta_x}{J}\frac{\partial \boldsymbol{E}}{\partial \eta} + \frac{\eta_y}{J}\frac{\partial \boldsymbol{F}}{\partial \eta} = 0 \tag{7}$$

The momentum equations in this form are expanded as finite differences about the node at $(i+1,j)$ in the computational plane. The differencing method employed for each of the terms within the flux vectors $\boldsymbol{E}$ and $\boldsymbol{F}$ is described later. The primary values used in the difference equations are shown schematically in Fig. 2.

The streamwise convective terms are upwinded to produce a positive coefficient on the implicit term at node $(i+1,j)$. To minimize numerical dissipation, the second-order upwind method is used primarily, except adjacent to boundaries. For streamwise flow in the marching direction, the upstream terms are currently known from the solution at previous stations. In regions of reversed flow, the grid direction of the differencing is reversed, and the convective flux terms at the downstream nodes are lagged.

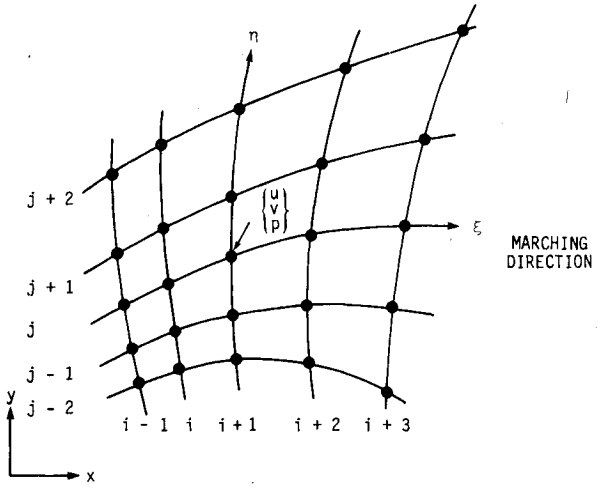

Fig. 1 General nonorthogonal curvilinear coordinate grid.

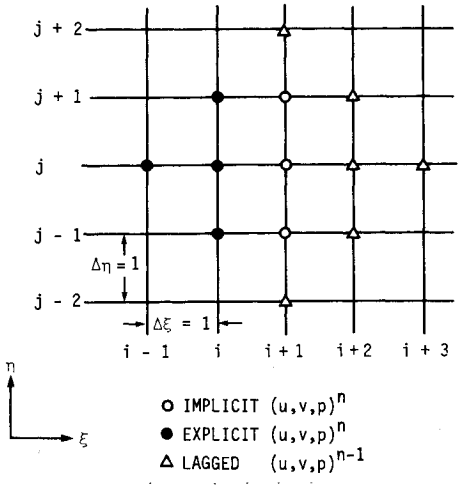

Fig. 2 Momentum equation finite-difference molecule at $(i+1,j)$.

The hybrid differencing scheme is used for the transverse convective terms. Central differencing is used for mesh Reynolds numbers less than 2. For larger mesh Reynolds numbers, the differencing is progressively weighted toward the first-order upwind scheme. These terms at station $i+1$ are implicit.

The streamwise pressure gradient is forward differenced to produce a negative coefficient on the implicit term at node $(i+1,j)$. Although a second-order forward difference expresion is applied easily, the results presented here were obtained with a first-order representation. The downstream pressure values are the estimated values resulting from the global pressure correction procedure following the previous iteration. The first-order forward difference at $(i+1,j)$ is

$$p_\xi = (\bar{p}^n_{i+2,j} - p^n_{i+1,j})/\Delta\xi \tag{8}$$

Central differencing of the transverse pressure gradient was found to permit the even and odd node pressures to uncouple, producing two independent profiles at some stations. Therefore, to link the pressures at neighboring nodes, one-sided, second-order differences are used. The three-point difference formulas include nodes outside the bandwidth of the block-tridiagonal solver. Rather than use a pentadiagonal solver, the second-order expression is split into an implicit first-order term plus an explicit second-order correction based on the estimated pressure field. The second-order forward difference formula about $(i+1,j)$ is

$$p_\eta = (p^n_{i+1,j+1} - p^n_{i+1,j})/\Delta\eta - (\bar{p}^n_{i+1,j} - 2\bar{p}^n_{i+1,j+1} + \bar{p}^n_{i+1,j+2})/2\Delta\eta \tag{9}$$

Second-order central differences are used for the viscous terms. The transverse terms are all implicit. The downstream values in the streamwise and mixed partial derivatives are lagged.

Continuity Equation

The governing equations [Eq. (1)] can be transformed and expressed in strong-conservation-law form as

$$\frac{\partial \boldsymbol{E}'}{\partial \xi} + \frac{\partial \boldsymbol{F}'}{\partial \eta} = 0 \tag{10}$$

where

$$\boldsymbol{E}' = (\xi_x/J)\boldsymbol{E} + (\xi_y/J)\boldsymbol{F}, \qquad \boldsymbol{F}' = (\eta_x/J)\boldsymbol{E} + (\eta_y/J)\boldsymbol{F}$$

The continuity equation is expanded in the finite-volume form of Eq. (10) to give

$$(E'_e - E'_w)/\Delta\xi + (F'_n - F'_s)/\Delta\eta = 0 \tag{11}$$

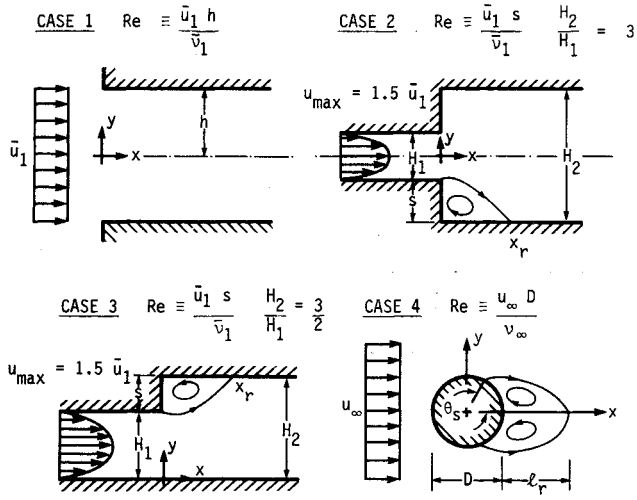

Fig. 3 Test case flow geometries.

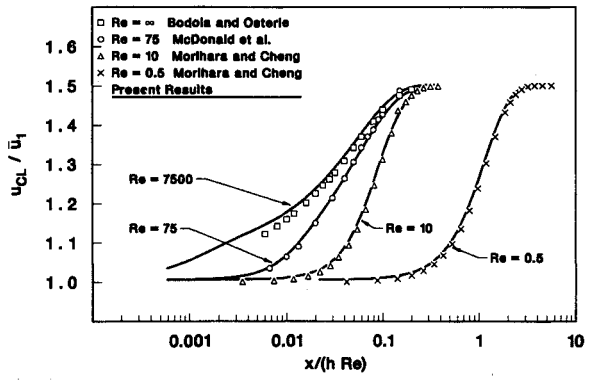

Fig. 4 Predicted centerline velocity distribution for developing flow in a two-dimensional channel inlet.

Here, the subscripts denote the faces of the resulting control volume centered at $(i+\frac{1}{2},j)$. Substituting the fluxes and dropping $\Delta\xi=\Delta\eta=1$ gives

$$\left(\frac{\rho U}{J}\right)_e-\left(\frac{\rho U}{J}\right)_w+\left(\frac{\rho V}{J}\right)_n-\left(\frac{\rho V}{J}\right)_s=0 \tag{12}$$

where the contravariant velocities are

$$U=(\xi_x u+\xi_y v), \qquad V=(\eta_x u+\eta_y v)$$

The east and west face fluxes are obtained directly at the nodes $(i+1,j)$ and (i,j) in the center of these faces. However, the fluxes at the centers of the north and south faces at $(i+\frac{1}{2},j+\frac{1}{2})$ and $(i+\frac{1}{2},j-\frac{1}{2})$ must be interpolated. Simple averaging among the four neighboring nodes leads to a central difference expression that causes even/odd decoupling and produces sawtooth profiles. To suppress this, the interpolation is done by a Taylor expansion biased to one side of the control volume center. Second-order accuracy is maintained, but some dissipation error is introduced into the equation. The direction of the transverse differencing is opposite the one-sided differencing of the transverse pressure gradient in the momentum equations. For example, the north face flux terms are determined from the properties and gradients about the node at $(i+1,j)$ as

$$(\rho u)_n=(\rho u)_{i+1,j}+\frac{\Delta\eta}{2}\left[\frac{\partial}{\partial\eta}(\rho u)\right]_{i+1,j}-\frac{\Delta\xi}{2}\left[\frac{\partial}{\partial\xi}(\rho u)\right]_{i+1,j} \tag{13}$$

Expanding the derivatives gives

$$(\rho u)_n=(\rho u)^n_{i+1,j}+\tfrac{1}{2}\left[(\hat{\rho}\hat{u})_{i+1,j}-(\hat{\rho}\hat{u})_{i+1,j-1}\right]-\tfrac{1}{4}\left[(\hat{\rho}\hat{u})_{i+1,j}-(\hat{\rho}\hat{u})_{i-1,j}\right] \tag{14}$$

The south face flux is then determined about the corresponding node at $(i+1,j-1)$ in a similar manner. To maintain the block-tridiagonal matrix, the correction terms are explicit and lagged within the nonlinear coefficient loop.

The metric terms for each face represent the control volume face areas. In order to insure strict flux conservation, the metrics must satisfy the geometric conservation law. As an example, the metrics used for the north face are

$$\left(\frac{\eta_x}{J}\right)_n=(y_\xi)_n=(y_{i,j+\frac{1}{2}}-y_{i+1,j+\frac{1}{2}})/\Delta\xi \tag{15a}$$

$$\left(\frac{\eta_y}{J}\right)_n=(x_\xi)_n=(x_{i+1,j+\frac{1}{2}}-x_{i,j+\frac{1}{2}})/\Delta\xi \tag{15b}$$

This treatment of the metrics reproduces the areas of the physical coordinate continuity control volume. The transformed difference equation is equivalent to a finite-volume continuity equation in physical coordinate form.

Boundary Conditions

The space-marching pass starts from the upstream boundary where the inlet flow profile is specified. It is notable that since the streamwise pressure gradient terms in the momentum equations are forward differenced, the upstream boundary pressure influences the flow solution only through the density.

On solid walls u and v are zero, and the normal pressure gradient is set equal to zero. At freestream side boundaries u and p are set equal to freestream values, and continuity requirements establish v.

The set of governing equations is solved at the downstream boundary assuming zero streamwise diffusion. The downstream pressure is specified one step outside of the grid. For external flows, the downstream pressure is equal to the freestream pressure. For internal flows, the value of the downstream pressure is adjusted between iterations in order to impose a total pressure drop from the inlet reference pressure consistent with the specified mass flowrate.

Solution of the Block-Tridiagonal System

The difference equations and the boundary conditions at station $i+1$ form a block-tridiagonal system of equations for q. However, the convective flux terms in both the momentum and continuity equations are nonlinear. These terms are quasilinearized in terms of q about coefficient values lagged from the previous global iteration. Examples of the quasilinearized terms are (the caret denotes coefficient values)

$$\rho u\approx\left[\hat{\rho}\left(1+\frac{\hat{u}^2}{c_p\hat{T}}\right)\right]u+\left[\frac{\hat{\rho}\hat{u}\hat{v}}{c_p\hat{T}}\right]v+\left[\frac{\hat{u}}{R\hat{T}}\right]p-\left[\hat{\rho}\hat{u}\left(1+\frac{\hat{u}^2+\hat{v}^2}{c_p\hat{T}}\right)\right] \tag{16}$$

$$\rho u^2\approx\left[\hat{\rho}\hat{u}\left(2+\frac{\hat{u}^2}{c_p\hat{T}}\right)\right]u+\left[\frac{\hat{\rho}\hat{v}\hat{u}^2}{c_p\hat{T}}\right]v+\left[\frac{\hat{u}^2}{R\hat{T}}\right]p-\left[\hat{\rho}\hat{u}^2\left(2+\frac{\hat{u}^2+\hat{v}^2}{c_p\hat{T}}\right)\right] \tag{17}$$

The linear system is easily solved by a block elimination procedure. When the solution results in a large change in the variables, the quasilinearization is repeated about the new values

Table 1 Summary of test case parameters

Case	Inlet profile	Re	M_1	L[a]	x_1/L	x_2/L	Grid	ITN[b]	ϵ_{max}	α	ω
1	uniform u	7500	0.01	h	0	3000	41×21	7	10^{-4}	20	0.7
	$v=0$	75	0.01		0	30	41×21	17	10^{-4}	20	0.7
		10	0.01		0	4	41×21	60	10^{-4}	5	0.7
		0.5	0.01		0	2	41×21	183	10^{-4}	5	0.7
2	parabolic u	37.3	0.05	s	−3	12	[c]	[c]	10^{-6}	80	0.5
	$v=0$										
3	parabolic u	229	0.05	s	−6	48	[c]	[c]	10^{-6}	80	0.5
	$v=0$	73	0.05		−6	24	[c]	[c]	10^{-6}	80	0.5
4	uniform u	40	0.05	D	−20	20	41×21	263	10^{-4}	10	0.1
	$v=0$				−20	20	81×41	486	10^{-4}	80	0.1

[a] See Fig. 3. [b] ITN = Number of global iterations. [c] See Table 2.

and the system is subsequently solved using the updated coefficients. For the test cases presented here, iteration on the nonlinear coefficients was not typically required at most of the marching stations.

Global Pressure Correction Procedure

An auxiliary Poisson equation for the pressure field can be obtained by a linear combination of derivatives of the momentum equations as

$$p_{\xi\xi} + \alpha p_{\eta\eta} = Sp \tag{18}$$

where α is an arbitrary constant and $Sp = (p_\xi)_\xi + \alpha(p_\eta)_\eta$. The pressure gradients in the source term are determined from the momentum equations. The solution of an approximate form of Eq. (18) between marching sweeps is used to estimate a corrected pressure field that accelerates convergence.

In the present space-marching formulation, two pressure values are used: the calculated pressure p^n, and the assumed pressure field $\bar{p}^n$, which provides the downstream pressure needed for stable marching. At an intermediate iteration n, let the difference between the calculated pressure and the assumed pressure be defined as

$$\epsilon^n_{i,j} = p^n_{i,j} - \bar{p}^n_{i,j}$$

Let the difference between the final converged pressure and the assumed pressure be defined as

$$\delta^n_{i,j} = p^\infty_{i,j} - \bar{p}^n_{i,j}$$

At convergence, δ and ϵ approach zero at all points in the field.

If δ could be determined exactly, then the ideal pressure correction would be

$$\bar{p}^{n+1}_{i,j} = \bar{p}^n_{i,j} + \delta^n_{i,j} \tag{19}$$

Substitution of the definition of δ into Eq. (18) gives a Poisson equation in terms of the pressure correction.

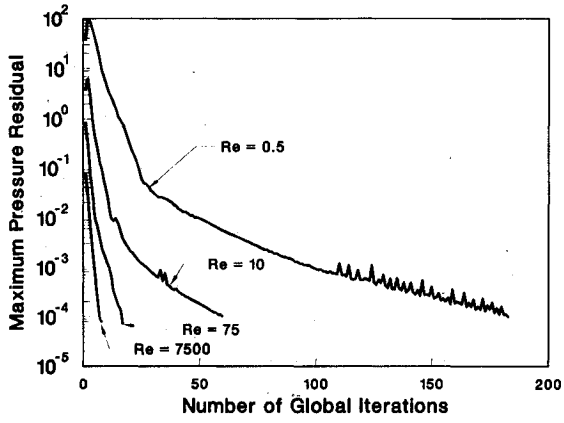

Fig. 5 Convergence history of channel inlet solutions.

$$(\bar{p}^n_{\xi\xi} + \delta^n_{\xi\xi}) + \alpha(\bar{p}^n_{\eta\eta} + \delta^n_{\eta\eta}) = Sp \tag{20}$$

The current space-marched solution directly provides a good estimate of the local pressure gradients in the source term. Expanding the source term at $(i+1,j)$ gives

$$Sp \approx \left[(\bar{p}^n_{i+2,j} - p^n_{i+1,j}) - (\bar{p}^n_{i+1,j} - p^n_{i,j})\right]/\Delta\xi^2 + \alpha\left[(p^n_{i+1,j+1} - p^n_{i+1,j}) - (p^n_{i+1,j} - p^n_{i+1,j-1})\right]/\Delta\eta^2 \tag{21}$$

However, solving the elliptic equation (20) would require substantial computational effort. To simplify Eq. (20), it is assumed that the pressure gradient term upstream of node $(i+1,j)$ will be corrected to the current solution value as

$$\bar{p}^{n+1}_{i+1,j} - \bar{p}^{n+1}_{i,j} \approx \bar{p}^n_{i+1,j} - p^n_{i,j} \tag{22}$$

Expanding Eq. (20) with the standard central difference representation of the second derivatives, using Eqs. (21) and (22), and applying the definitions of ϵ and δ leaves a parabolic difference equation for δ.

$$\alpha\delta^n_{i+1,j-1} - (1+2\alpha)\delta^n_{i+1,j} + \alpha\delta^n_{i+1,j+1} = \alpha\epsilon^n_{i+1,j-1} - (1+2\alpha)\epsilon^n_{i+1,j} + \alpha\epsilon^n_{i+1,j+1} - \delta^n_{i+2,j} \tag{23}$$

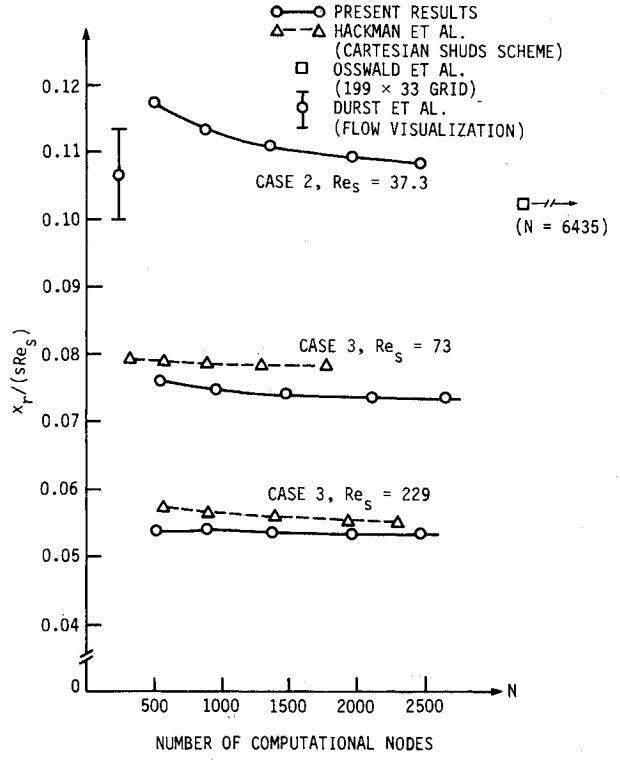

Fig. 6 Effect of grid refinement on predicted reattachment length for sudden expansion flow in a two-dimensional channel.

Table 2 Results of grid refinement for sudden expansion flow cases

Grid indices		Results		
I_{MAX}	J_{MAX}	N[a]	Xr/s	ITN[b]
Case 2, $Re_s = 37.3$				
31	19	517	4.384	21
41	25	897	4.232	20
51	31	1381	4.142	21
61	37	1969	4.086	23
71	40	2476	4.048	27
Case 3, $Re_s = 73$				
31	19	553	5.550	33
41	25	961	5.465	31
51	31	1481	5.414	27
61	37	2113	5.386	25
71	40	2658	5.362	24
Case 3, $Re_s = 229$				
28	19	514	12.31	34
37	25	893	12.35	31
46	31	1376	12.26	30
55	37	1963	12.22	28
64	40	2469	12.22	29

[a] N = Number of nodes. [b] ITN = Number of global iterations.

Table 3 Iterations required for case 3 at $Re_s = 229$ with a 46×31 uniform grid

Diffusion factor, α	Relaxation factor, ω			
	0.100	0.250	0.500	0.707
10	108	a	a	a
20	106	48	a	a
40	103	50	35	a
80	141	58	30	26
120	197	73	31	29
200	305	103	42	a
400	525	157	64	a

[a] Solution diverges.

Table 4 Separation bubble predictions for case 4, $Re_D = 40$

	θ_s, deg	ℓ_r/D
Son and Hanratty[25]	53.9	2.5
Present results	52.7	2.38
Rhie[26]	—	2.07
Kwak et al.[8]	52.0	1.9

For compactness, the terms $\Delta\xi = \Delta\eta = 1$ have been eliminated. Since there is no correction to the specified pressure at the far downstream boundary, Eq. (23) can be solved for δ at each station by a single backsweep using a tridiagonal line solver. The scheme rapidly transmits pressure changes in the upstream direction. Excessive skewing of the transverse pressure profiles is prevented by diffusion of the streamwise pressure changes across grid lines. The magnitude of the diffusion factor α controls the degree to which the transverse pressure profiles are preserved. Under-relaxation of the predicted pressure correction is needed, and so the actual pressure correction applied is

$$\bar{p}_{i,j}^{n+1} = \bar{p}_{i,j}^{n} + \omega\delta_{i,j}^{n} \tag{24}$$

The computational effort to execute the procedure is insignificant compared to the space-marching solution of the coupled governing equations.

Results

Sample results are presented for four test cases. The geometry for each case is shown in Fig. 3. The flow conditions and several grid and iteration parameters are listed in Table 1. All solutions, with the exception of the fine grid computation of case 4, were started assuming a uniform pressure field and zero velocity. The computations were performed on an Intel 8088/8087 microprocessor-based personal computer and checked on a VAX 11/785. The CPU time on the VAX was approximately 0.006 s per node per iteration.

The test cases present different aspects of elliptic flow problems. First, the entrance flow in a channel at low Reynolds number induces a complex pressure and velocity field that differs from the high Reynolds number flow. Next, the sudden expansion geometries produce recirculation regions. Finally, the crossflow over a cylinder includes a stagnation point, separated flow, and large streamline curvature and was computed on a nonorthogonal grid. Incompressible flow is simulated by prescribing a low Mach number ($M < 0.1$).

Developing Flow in a Channel

The entrance flow in a channel with an arbitrarily imposed uniform inlet profile is labeled as case 1. Solutions were calculated on the channel upper half-plane using a rectangular grid with lines packed near the inlet plane and the wall. The marching direction step size varied from 0.00145 to 0.0664 of the channel length, and the transverse grid spacing ranged from 0.0125 to 0.0901 of the channel half-width. The predicted centerline velocity distributions are shown in Fig. 4 along with the numerical results of previous investigators.[18-20] Good agreement was achieved for all Reynolds numbers.

The convergence histories for the calculations are shown in Fig. 5. The most rapid convergence was observed for the higher Reynolds number cases. For the low Reynolds number runs, the convergence rate diminished as convergence was approached. Possible causes of this behavior are the following: 1) slow convergence of the streamwise diffusion terms that depend on downstream velocities and 2) the singularity at the inlet corner (see Ref. 21). For this computational test case, the inlet flow profile was arbitrarily specified to be uniform to allow comparison with other solutions. However this profile is inconsistent with real flow; an artificially high pressure was calculated at the corner that would normally propagate upstream and alter the inlet flow. The computed pressure spike is larger for lower Reynolds numbers and may be a cause of the slower convergence.

Sudden Expansion Flow in a Channel

The symmetric 3/1 sudden expansion flow in a channel is labeled as case 2. Computations were performed on the channel upper half-plane with a series of uniform grids. Fully developed flow was assumed at the inlet plane located upstream of the expansion. The last marching station was placed downstream of the reattachment point where the downstream pressure is constant across the channel, but the flow was not assumed to be fully developed. A similar series of computations was done for the 3/2 asymmetric expansion flow labeled as

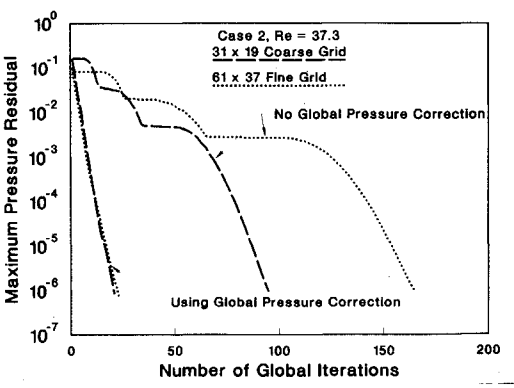

Fig. 7 Effect of global pressure correction on convergence history of symmetric sudden expansion solutions.

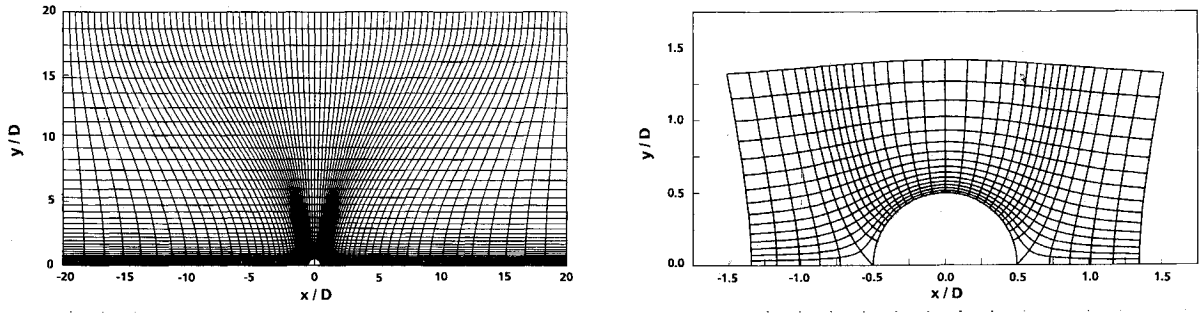

Fig. 8 Computational grid for case 4 with detail view of the region near the cylinder.

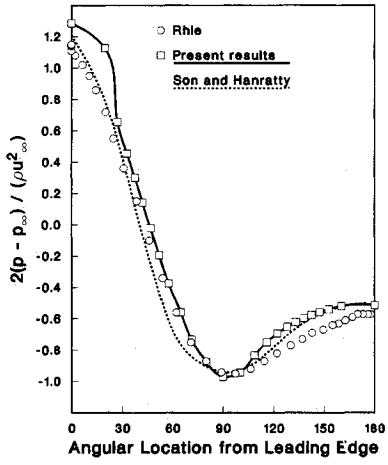

Fig. 9 Predicted surface pressure distribution for crossflow over a cylinder at $Re_D = 40$.

case 3. The results of the grid refinement tests are summarized in Table 2. The predicted reattachment lengths are compared with the experimental result of Durst et al.[22] and the numerical predictions of Osswald et al.[23] and Hackman et al.[24] in Fig. 6. Reasonable accuracy is demonstrated, even with fairly coarse grids.

For these cases, the convergence rate was not strongly dependent on the number of nodes or the Reynolds number, and rapid convergence was obtained on all runs. The convergence behavior was dependent on the choice of the diffusion and relaxation factors in the pressure correction procedure, as shown in Table 3. Low values for the diffusion parameter or large values of the relaxation factor cause the solution to immediately diverge. Very large values of the diffusion factor result in an oscillating or diverging solution. The procedure is stable with small values of the relaxation factor at a large penalty in the convergence rate. Based on limited experience with the method, the optimum values of these parameters appears to be problem dependent. Also, rather than holding these values fixed, the results of Bentson and Vradis[15] with a different pressure correction method suggest that varying the diffusion parameter during the course of the calculation may be beneficial.

To demonstrate the accelerating effect of the global pressure correction scheme, additional case 2 computations were done without using this procedure. Multiple space-marching passes were performed using only relaxation of the pressure to converge the solution. Figure 7 compares the convergence history for coarse and fine grid solutions done with and without the global pressure correction. Convergence is reached between 4 and 10 times faster with the global pressure correction scheme, depending on the grid and the convergence tolerance chosen.

Crossflow over a Cylinder

The crossflow over a cylinder is labeled as case 4. The nonorthogonal grid shown in Fig. 8 was constructed using the stream and potential functions for potential flow with stretching functions to cluster nodes near the body. The computed surface pressure distribution is compared in Fig. 9 with the numerical results of Son and Hanratty[25] and the more recent work of Rhie.[26] The pressure distribution is reasonably well predicted over most of the cylinder, except near the leading edge. The grid does not contain enough nodes near the stagnation point to accurately resolve the steep gradients in this area. It is believed that an improved computational grid would result in a more accurate prediction of the stagnation point pressure. Predictions of the separation point and the length of the trailing separation bubble are given in Table 4. The present predictions fall in the range between the results obtained by Kwak et al.[8] and Son and Hanratty.[25]

The convergence rate for this case was much slower than for the internal flow cases. Smaller relaxation factors were used and an exception to the starting procedure was made for the fine grid computation, which was started using interpolated values from the coarse grid solution. This was necessary due to the large obstruction presented by the cylinder leading edge. On the initial sweep, there is no deviation from uniform freestream conditions until the leading edge is encountered, and the flow must be diverted in the space of one grid step. If too fine a mesh is specified, an unrealistically large transverse velocity is required to pass the flow around the obstruction. The large perturbation at the leading-edge marching station may cause the Newton linearization to fail or the subsequent profiles downstream will be physically unrealistic and require that the pressure correction be very heavily relaxed.

Concluding Remarks

An efficient, coupled space-marching procedure has been developed for the full Navier-Stokes equations in primitive variables. The finite-difference method has been implemented on a regular grid using generalized body-fitted coordinates. Several comparisons have been made that confirm that the method correctly captures the global influences that characterize fully eliptic flows. The compressible formulation was observed to work very well in the incompressible limit. A new global pressure correction procedure was developed that significantly accelerates convergence for an important class of problems.

Acknowledgment

This material is based on work supported by the National Science Foundation under Grant CBT-8211713. The authors wish to thank Xuezong Liu for many helpful discussions during the formative stages of this work.

References

[1]Anderson, D. A., Tannehill, J. C., and Pletcher, R. H., *Computational Fluid Mechanics and Heat Transfer,* Hemisphere, New York, 1984.

[2]Patankar, S. V., "A Calculation Procedure for Two-Dimensional Elliptic Situations," *Numerical Heat Transfer,* Vol. 4, No. 4, 1981, pp. 409-426.

[3]Ghia, K. N., Hankey, W. L., Jr., and Hodge, J. K., "Use of Prim-

itive Variables in the Solution of Incompressible Navier-Stokes Equations," *AIAA Journal,* Vol. 17, No. 3, 1979, pp. 298–301.

[4]Rhie, C. M., "A Pressure Based Navier-Stokes Solver Using the Multigrid Method," AIAA Paper 86-0207, Jan. 1986.

[5]Van Doormaal, J. P., Turan, A., and Raithby, G. D., "Evaluation of New Techniques for the Calculation of Internal Recirculating Flows," AIAA Paper 87-0059, Jan. 1987.

[6]Vanka, S. P., and Leaf, G. K., "Fully-Coupled Solution of Pressure-Linked Fluid Flow Equations," Argonne National Laboratory, Rept. ANL-83-73, Aug. 1983.

[7]Patankar, S. V., Karki, K. C., and Mongia, H. C., "Development and Evaluation of Improved Numerical Schemes for Recirculating Flows," AIAA Paper 87-0061, Jan. 1987.

[8]Kwak, D., Chang, J. L. C., Shanks, S. P., and Chakravarthy, S. R., "An Incompressible Navier-Stokes Flow Solver in Three-Dimensional Curvilinear Coordinate System Using Primitive Variables," *AIAA Journal,* Vol. 24, No. 3, 1986, pp. 390–396.

[9]Chorin, A. J., "A Numerical Method for Solving Incompressible Viscous Flow Problems," *Journal of Computational Physics,* Vol. 2, No. 1, 1967, pp. 12–26.

[10]Beam, R. M., and Warming, R. K., "An Implicit Finite-Difference Algorithm for Hyperbolic Systems in Conservation-Law Form," *Journal of Computational Physics,* Vol. 22, Sept. 1976, pp. 87–110.

[11]Rubin, S. G., and Reddy, D. R., "Analysis of Global Pressure Relaxation for Flows with Strong Interaction and Separation," *Computers & Fluids,* Vol. 11, No. 4, 1983, pp. 281–306.

[12]Israeli, M., and Lin, T., "Iterative Numerical Solutions and Boundary Conditions for the Parabolized Navier-Stokes Equations," *Computers and Fluids,* Vol. 13, No. 4, 1985, pp. 397–410.

[13]Pougare, M., and Lakshminarayana, B., "A Space-Marching Method for Incompressible Navier-Stokes Equations," AIAA Paper 85-0170, Jan. 1985.

[14]Liu, X., and Pletcher, R. H., "A Coupled Marching Procedure for the Partially Parabolized Navier-Stokes Equations," *Numerical Heat Transfer,* Vol. 10, No. 6, 1986, pp. 539–556.

[15]Bentson, J., and Vradis, G., "A Two-Stage Pressure Correction Technique for the Incompressible Navier-Stoies Equations," AIAA Paper 87-0545, Jan. 1987.

[16]Vigneron, Y. C., Rakich, J. V., and Tannehill, J. C., "Calculation of Supersonic Viscous Flow over Delta Wings with Sharp Subsonic Leading Edges," AIAA Paper 78-1137, July 1978.

[17]Hindman, R. G., "Generalized Coordinate Forms of Governing Fluid Equations and Associated Geometrically Induced Errors," *AIAA Journal,* Vol. 20, No. 10, 1982, pp. 1359–1367.

[18]Bodoia, J. R., and Osterle, J. F., "Finite Difference Analysis of Plane Poiseuille and Couette Flow Development," *Applied Scientific Research,* Vol. 10, Sec. A, No. 3-4, 1961, pp. 265–276.

[19]McDonald, J. W., Denny, V. E., and Mills, A. F., "Numerical Solutions of the Navier-Stokes Equations in Inlet Regions," *Journal of Applied Mechanics,* Vol. 39, Series E, Dec. 1972, pp. 873–878.

[20]Morihara, H., and Cheng, R. T., "Numerical Solution of the Viscous Flow in the Entrance Region of Parallel Plates," *Journal of Computational Physics,* Vol. 11, No. 4, 1973, pp. 550–572.

[21]Van Dyke, M., "Entry Flow in a Channel," *Journal of Fluid Mechanics,* Vol. 44, No. 4, 1970, pp. 813–823.

[22]Durst, F., Melling, A., and Whitelaw, J. H., "Low Reynolds Number Flow over a Plane Symmetric Sudden Expansion," *Journal of Fluid Mechanics,* Vol. 64, No. 1, 1974, pp. 111–128.

[23]Osswald, G. A., Ghia, K. N., and Ghia, U., "Unsteady Navier-Stokes Simulation of Internal Separated Flows over Plane and Axisymmetric Sudden Expansions," AIAA Paper 84-1584, June 1984.

[24]Hackman, L. P., Raithby, G. D., and Strong, A. B., "Numerical Prediction of Flow over Backward-Facing Steps," *International Journal of Numerical Methods in Fluids,* Vol. 4, 1984, pp. 711–724.

[25]Son, J. S., and Hanratty, T. J., "Numerical Solution for the Flow Around a Circular Cylinder at Reynolds Number of 40, 200, and 500," *Journal of Fluid Mechanics,* Vol. 35, No. 2, 1969, pp. 369–386.

[26]Rhie, C. M., "A Numerical Study of the Flow Past an Isolated Airfoil with Separation," Ph.D. Dissertation, Univ. of Illinois, Urbana, IL, 1981.